

Article

Experimental Studies of Combustion and Emission Characteristics of Biomass Producer Gas (BPG) in a Constant Volume Combustion Chamber (CVCC) System

Jun Sheng Teh ¹, Yew Heng Teoh ^{1,*} , Heoy Geok How ², Mohamad Yusof Idroas ¹, Thanh Danh Le ^{3,*} and Huu Tho Nguyen ⁴

¹ School of Mechanical Engineering, Engineering Campus, Universiti Sains Malaysia, Nibong Tebal 14300, Penang, Malaysia

² Department of Engineering, School of Engineering, Computing and Built Environment, UOW Malaysia KDU Penang University College, 32 Jalan Anson, Georgetown 10400, Penang, Malaysia

³ Faculty of Mechanical Engineering, Industrial University of Ho Chi Minh City, 12 Nguyen Van Bao Street, Ward 4, Go Vap District, Ho Chi Minh City 70000, Vietnam

⁴ Department of Fundamentals of Mechanical Engineering, Faculty of Engineering and Technology, An Phu Dong Campus 2, Nguyen Tat Thanh University, 1165 National Route 1A, An Phu Dong Ward, District 12, Ho Chi Minh City 729800, Vietnam

* Correspondence: yewhengteoh@usm.my (Y.H.T.); lethanhdanh@iuh.edu.vn (T.D.L.)

Abstract: Most of the world's energy requirements are still derived from natural resources. This will result in a catastrophic energy crisis with negative environmental consequences. The increased energy supply will result in greater consumption of non-renewable sources. The production of biomass producer gas (BPG) from biomass gasification has received significant attention as an alternative fuel due to the depletion of non-renewable resources. This experimental study aimed to determine the flame propagation, flame propagation speed, and chamber pressure trace of BPG at different equivalence ratios. Understanding the characteristics of the BPG's combustion, finding lower greenhouse gas emissions of BPG, and minimizing the use of fossil fuels is necessary to mitigate these problems. Using the direct visualization technique, an optical constant volume combustion chamber (CVCC) was developed to measure combustion characteristics. Liquid petroleum gas (LPG) was used to compare the flame propagation speed in the CVCC calibration. In comparison to wood pellet (WP), coconut husk (CH), and palm kernel shell (PKS), the chamber peak pressure at ϕ equal to 1 of CH for the combustion of BPG was the lowest at 20.84 bar. At ϕ of 0.7, 0.8, 0.9, 1.0, 1.1, 1.2, and 1.3, the chamber peak pressure of CH was discovered to be around 17.77, 18.12, 18.81, 20.84, 20.39, 17.25, and 16.37 bar, respectively. Compared to the other two types of BPG, CH produced the lowest emissions of CO₂ and CO at 2.03% and 0.022%, respectively. In conclusion, the CH had the lowest chamber peak pressure and emissions due to the lower heating value (LHV) being relatively lower.

Keywords: renewable energy; biomass producer gas; constant volume combustion chamber; flame propagation; chamber pressure; emission



Citation: Teh, J.S.; Teoh, Y.H.; How, H.G.; Idroas, M.Y.; Le, T.D.; Nguyen, H.T. Experimental Studies of Combustion and Emission Characteristics of Biomass Producer Gas (BPG) in a Constant Volume Combustion Chamber (CVCC) System. *Energies* **2022**, *15*, 7847. <https://doi.org/10.3390/en15217847>

Academic Editors: Luca Cioccolanti and Luca Del Zotto

Received: 28 September 2022

Accepted: 19 October 2022

Published: 23 October 2022

Publisher's Note: MDPI stays neutral with regard to jurisdictional claims in published maps and institutional affiliations.



Copyright: © 2022 by the authors. Licensee MDPI, Basel, Switzerland. This article is an open access article distributed under the terms and conditions of the Creative Commons Attribution (CC BY) license (<https://creativecommons.org/licenses/by/4.0/>).

1. Introduction

Most of the world's energy requirements are still derived from natural resources. This will result in a catastrophic energy crisis with negative environmental consequences. The increased energy supply will result in greater consumption of non-renewable sources. Furthermore, fossil fuel burning emits significant greenhouse gases (GHG) such as sulfur dioxide (SO₂), nitrogen oxides (NO_x), and other harmful gases or contaminants, which contribute to the formation of smog and acid rain [1].

The main methods for converting biomass into energy are thermo-chemical and biological processes [2]. The five thermo-chemical conversion processes for biomass resources are

pyrolysis, combustion, gasification, hydrothermal liquefaction, and torrefaction [3]. Gasification of fossil fuels is a typical process in the biomass process for the production of BPG [4]. In the thermo-chemical process known as gasification, solid biomass is treated with a small amount of gasifying medium to produce a biomass producer gas (BPG) such as hydrogen (H_2), carbon dioxide (CO_2), methane (CH_4), or carbon monoxide (CO). The gasification process generates heat in an oxygen-poor atmosphere [5]. Woody biomass with low moisture content, such as spruce, pine, and alder, can be gasified to produce gas in a partial oxidation environment at temperatures ranging from 600 to 1400 °C [6]. The residual 30% feedstock mass and 10% biomass energy are discharged as liquids and gases, whereas 70% of the raw material mass and nearly 90% of the initial biomass energy are retrieved [7]. Gasification is a variable procedure easily influenced by the biomass mechanism, particle size, humidity, and equivalence ratio (ϕ), among other factors [8]. Additionally, a medium for the reaction is required, such as air, oxygen, subcritical steam, or various gaseous combinations [9]. The producer gases can be further transformed into liquid fuels through the Fischer–Tropsch process or by generating heat and energy for power plants [10]. Awais et al. [11] examined the co-gasification efficiency, reactor thermal profiles, and ϕ for a downdraft gasifier's specific yield of syngas composition and tar contents. The experimental results revealed that the syngas yield improved from 1.1 to 2.0 Nm^3/kg biomass and the ϕ increased from 0.18 to 0.30. During co-gasification, the temperature was typically between 800 and 875 °C. Under the gasifier, the gasification reaction took place. Thus, the gasifier was a significant variable that affected the gasification reaction [12]. In order to maximize the production of hydrogen, Ahmed et al. [13] investigated the biomass gasification process and subsequent optimization while taking into account several variables including the type of feedstock and gasifying agent. According to the experimental findings, when the hydrogen fraction was optimized, the steam-only gasification yield of hydrogen generation from the blended biomass feedstock reached a high percentage of 5.23% while the oxygen/steam gasification yield climbed from 1.63% to 5.22%. In a study by Michael et al. [14], various feedstocks were used in the experimental studies of a ferrocement downdraft gasifier (FDG) connected to a 20 kW engine. The higher moisture content caused the water vapor emitted from the drying and pyrolysis zone to condense on the cement downdraft gasifier and flow to the oxidation zone and extinguish the combustion process. Furthermore, the higher feedstock heating value had a considerable impact on gasification rates. As a result, bamboo and teak with energy contents greater than 28 MJ/kg caused the gasifier reactor's temperature to rise. The greatest producer gas flowrate and gasification temperature were 56 Nm^3/h and 1090 °C, respectively.

The combustion process involves hundreds of chemical reactions and many types of turbulence and acoustic field. The combustion process is further complicated by a complicated geometry and operating technique. In order to investigate various facets of the combustion process, several fundamental research issues were introduced, including flame propagation and speed. Endoscopy techniques and endoscopes were initially designed for medical applications but now can be used to visualize combustion and fuel spray patterns in challenging environments such as the optical engine and combustion chamber [15]. Wen et al. [16] employed a schlieren apparatus to analyze landfill gas flame propagation properties in a CVCC. The trials were carried out with methane concentrations of 47%, 55.5%, and 59%; an ϕ range of 0.7 to 1.4; a pressure range of 0.1 to 0.5 MPa; and a temperature range of 290 to 380 K. The experimental data demonstrated that as the ϕ grew, the laminar combustion velocity and unstretched flame velocity initially increased and then gradually declined; the maximum values were measured when the ϕ was 1.1. Furthermore, with a higher initial pressure or lower initial temperature and methane content, the laminar combustion velocity of the landfill gas was reduced. Wang et al. [17] assessed direct-injected methanol ignited by diesel using shadowgraph and natural luminescence imaging in a CVCC that allowed both fuels to be directly injected at high pressure. The findings indicated that the pilot methanol and diesel injection combination ignited a fire in the diesel-rich area and that the flame propagated promptly along the jet's course before spreading slowly to

the methanol-rich area's periphery. On the one hand, this was primarily caused by the low cetane number of methanol, which makes it difficult to ignite. Agarwal et al. [18] discovered that chamber combustion photos could be captured using an endoscope with a viewing angle of 70° along its axis. Wang et al. [17] examined a procedure on a beam of homogeneous and parallel light that could be created and passed via the CVCC optical windows in this imaging system. The direct visualization technique was essential for visualizing the combustion process.

Chia-Fon Lee et al. [19] conducted a study of the compressed natural gas (CNG) substitution rates of 30%, 50%, 70%, and 85% (based on energy) on the premixed charge ϕ . Under conditions of various injector pressures and injected CNG/diesel amounts, Carlucci et al. [20] captured exhaust gas pressure and heat release rate (HRR) data and examined the composition and transparency of particular emissions. The research indicated that as more pilot fuel was injected, more heat was generated, which would cause the NO_x levels to drop and CO levels to rise. When the injection pressure was reduced, the CO levels rose while the NO_x levels dropped. According to numerous researchers, producer gas (PG) can be used in a single-fuel mode in SI engines [21,22]. Under full-load conditions, the modified SI engine employing producer gas had an efficiency of around 23 to 25% [23]. In addition, after proper pretreatment, the producer gas was admitted into the diesel engine combined with air through the air intake manifold. As a result of this fuel–air mixture input, less diesel injection was required for combustion and power generation. Consequently, it was possible to replace up to 90% of the diesel with the producer gas [24].

Since BPG has different combustion characteristics than diesel and gasoline, it is crucial to investigate the combustion characteristics of BPG. In this study, an alternate method for determining combustion characteristics employed a CVCC. The properties of the biomass feedstocks significantly influenced the combustion characteristics. Understanding the characteristics of BPG's combustion, finding lower greenhouse gas emissions of BPG, and minimizing the use of fossil fuels are necessary to mitigate these problems. Therefore, using direct visualization techniques, essential information about BPG combustion characteristics in a CVCC, such as the flame propagation, flame propagation speed, chamber pressure trace, gross heat release rate, and emissions of CO and CO_2 . These response parameters are essential in proposing the best strategies for controlling the combustion process of BPG.

2. Experimental Setup and Procedure

2.1. Biomass Feedstocks

In this experiment, three types of biomass feedstocks were considered, namely wood pellet (WP), coconut husk (CH), and palm kernel shell (PKS). The WP, CH, and PKS samples utilized in this experiment are shown in Figure 1 and their properties are listed in Table 1. The BPGs were collected and stored by utilizing a single-stage industrial gas compressor from a downdraft gasifier.

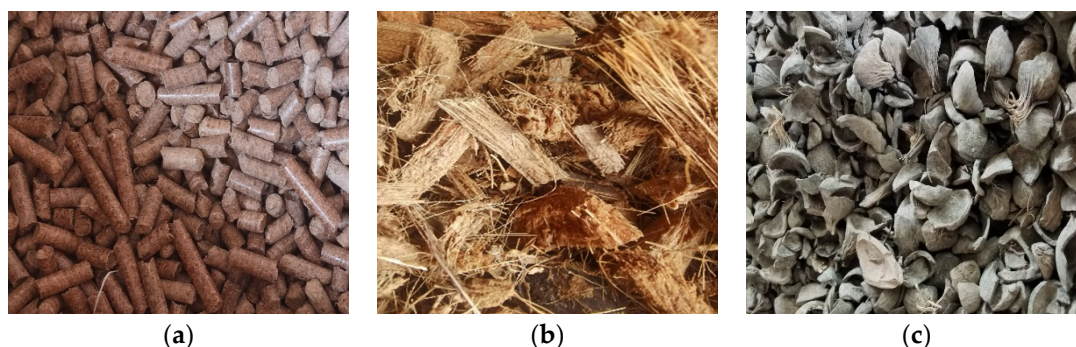


Figure 1. Biomass feedstocks used in the present study are (a) wood pellet, (b) coconut husk, and (c) palm kernel shell.

Table 1. The proximate and ultimate analysis of 3 biomass feedstocks.

Property	Wood Pellet	Coconut Husk	Palm Kernel Shell
Proximate Analysis			
Volatile matter (%)	78.89	69.99	61.26
Fixed carbon (%)	12.22	15.01	27.32
Ash (%)	0.83	0.53	2.83
Moisture content (%)	8.06	14.47	8.59
Ultimate Analysis			
Hydrogen (%)	3.41	1.65	1.78
Oxygen (%)	29.45	31.22	28.15
Nitrogen (%)	60.51	62.80	60.72
Carbon monoxide (%)	2.43	0.96	2.29
Methane (%)	0.77	0.45	0.4
Carbon dioxide (%)	2.43	2.93	6.67
LHV (MJ/Nm ³)	1	0.49	0.64
Density (kg/m ³)	1.23	1.22	1.26
AFR	1.7	1.59	1.65
Specific gas constant	310.35	284.38	280.1

2.2. Biomass Gasification

Figures 2 and 3 show the gasification apparatus used in this experiment. Gravity controlled the descent of the biomass through the gasifier's drying, pyrolysis, partial oxidation, and reduction zones. The gas was collected at the gasifier's bottom during the process. When the gasifier's emissions reached the cyclone, fly ash was created in the product gas. During the experiment process, the gasification was set to operate at a peak temperature of around 700 °C. In addition, gas chromatography was used to evaluate the BPGs collected after the gasification system's filter to determine the syngas concentration (H₂, O₂, N₂, CO, CH₄, and CO₂).

**Figure 2.** Setup of gasification.

2.3. Setup of CVCC

The experimental setup for BPG formation and measurement of combustion characteristics using the CVCC is shown in Figure 4. The CVCC's main body was fabricated from stainless steel and had an inner diameter of 118 mm, an outside diameter of 165 mm, and a thickness of 80 mm. A strata gas injector, pressure relief valve, and intake/exhaust ball valves were all included in the CVCC system. In the CVCC system, two spark ignition

probes were each assembled on the left and right of the chamber. The air gap (0.05 mm) between both spark ignition probes allowed an electric spark to pass between the conductors. To avoid an excessive pressure buildup inside the CVCC, a pressure relief valve was installed. In addition, a Kistler 6053B60 pressure sensor was employed to measure chamber pressure traces during the combustion process.

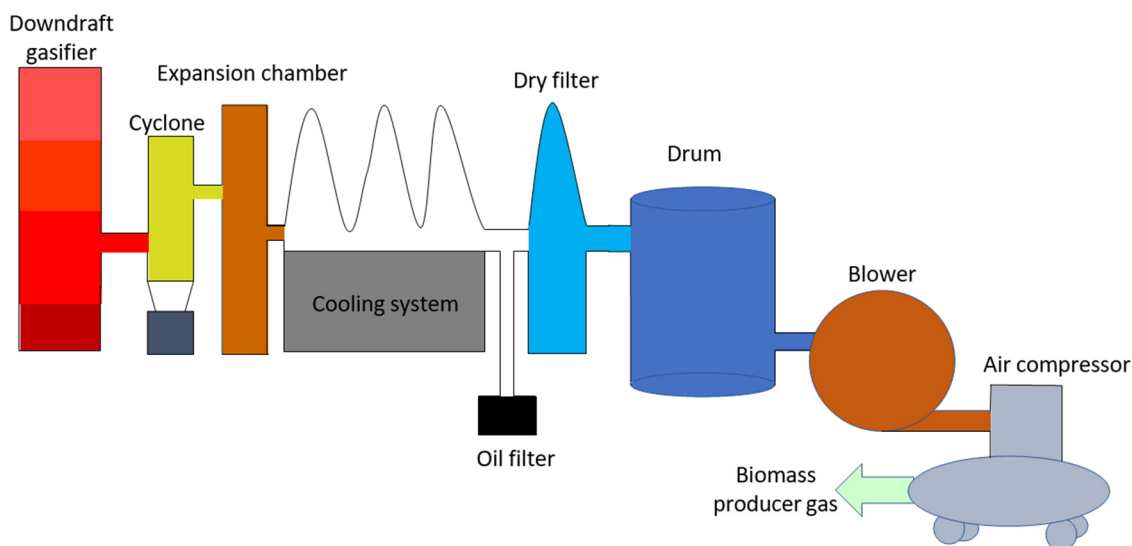


Figure 3. Scheme diagram of gasification.

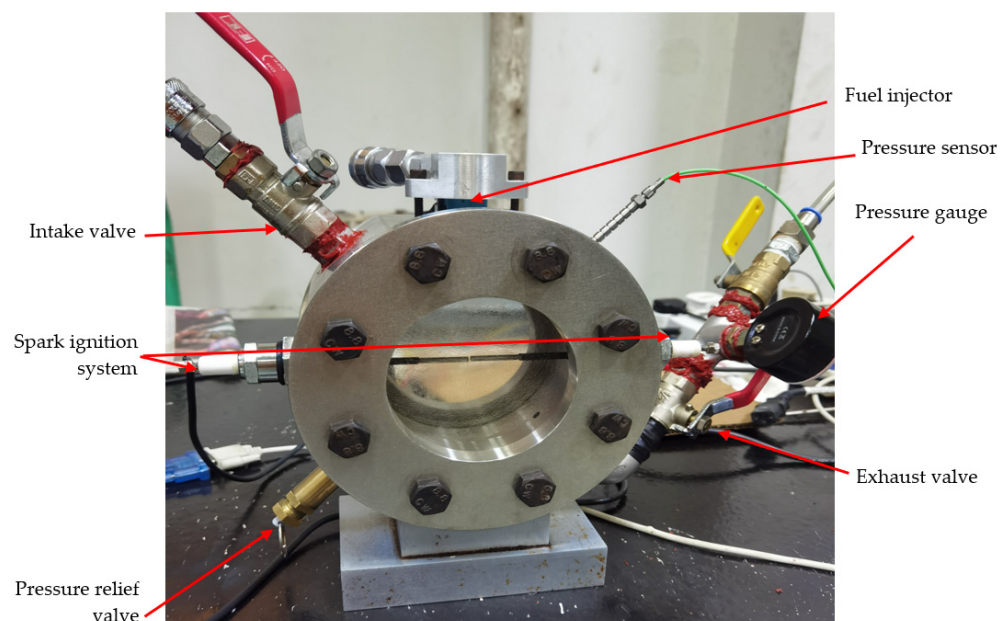


Figure 4. Setup of CVCC system.

A high-speed camera (model: Olympus I-Speed II) with a frame rate setting of 1000–2000 fps was used to capture the combustion reaction process inside the chamber. This allowed for a quick and easy way to record the combustion process. The recorded video from the high-speed camera could be visualized in real-time on the monitor. The flame speed was calculated using Equation (1), which showed the diameter scale of the flame during the combustion process. A pressure sensor was used to measure the chamber

pressure during the combustion process and NI-DAQ was used to acquire the behavior of each BPG based on the rate of pressure rise.

$$v_f = \frac{r_f}{t} \quad (1)$$

where v_f is flame propagation speed, r_f is the radius of the flame propagation, and t is the period during the combustion.

An essential parameter in determining the ϕ of a gas is its mass. For gases that do not dissolve in water, the mass flow rate of injection gas from the injector can be trapped in water using a method with water displacement. This technique requires a delivery tube, a measuring cylinder, and a water basin. Initially, the measuring cylinder is filled with water and inverted into a water basin. A delivery tube channels bubble gas into the inverted measuring cylinder. As gas bubbles and fills up the inverted measuring cylinder, the water level drops and the displaced water level corresponds to the gas volume measured at regular intervals. The pressure and airflow are constant for each injection to acquire the gas volume. The ideal gas law formula can be used to compute the mass of gas from the volume of gas:

$$d = \frac{P \times M}{R \times T} \quad (2)$$

$$m = d \times V \quad (3)$$

where d is the density of the gas, P is the pressure, M is the molar mass of the gas, R is the universal gas constant, T is the temperature, m is the mass of the gas, and V is the volume of the gas.

In this study, a ϕ of 0.7, 0.8, 0.9, 1.0, 1.1, 1.2, and 1.3 was examined for each fuel. Based on a fixed mass of BPG injected, the amount of air needed for each ϕ was estimated. Table 2 shows the mass of air and BPG injected at each ϕ for gaseous fuels was calculated using Equations (2) and (3). Table 3 displays a detailed list of the measurement equipment's type, range, accuracy, technique, and percentage of uncertainty.

Table 2. The calculation of the mass of air and BPG under various ϕ setting.

ϕ	Air Fuel Ratio	Mass of Air (g)	Mass of BPG (g)
LPG			
0.8	12.38	0.635	0.051
0.9	13.93	0.635	0.046
1.0	15.48	0.635	0.041
1.1	17.03	0.635	0.037
1.2	18.58	0.635	0.034
BPG (PKS)			
0.7	1.15	0.953	0.827
0.8	1.32	0.953	0.723
0.9	1.48	0.953	0.644
1.0	1.65	0.953	0.579
1.1	1.81	0.953	0.527
1.2	1.97	0.953	0.483
1.3	2.14	0.953	0.445
BPG (CH)			
0.7	1.12	0.953	0.854
0.8	1.28	0.953	0.747
0.9	1.43	0.953	0.664
1.0	1.59	0.953	0.598
1.1	1.75	0.953	0.543
1.2	1.91	0.953	0.598
1.3	2.07	0.953	0.460

Table 2. Cont.

ϕ	Air Fuel Ratio	Mass of Air (g)	Mass of BPG (g)
BPG (WP)			
0.7	1.19	0.953	0.798
0.8	1.36	0.953	0.699
0.9	1.53	0.953	0.621
1.0	1.70	0.953	0.559
1.1	1.88	0.953	0.508
1.2	2.05	0.953	0.466
1.3	2.22	0.953	0.430

Table 3. The type, range, accuracy, technique and percentage of uncertainty of the measuring equipment.

Measurement Type	Range	Accuracy	Techniques	% Uncertainty
Time	-	± 0.1 s	-	± 0.2
CO emission	0–10% Vol.	$\pm 0.01\%$ Vol.	Non-dispersive infrared	± 1
CO ₂ emission	0–10% Vol.	$\pm 0.01\%$ Vol.	Non-dispersive infrared	± 1
Pressure	0–2500 kPa	± 10 kPa	Piezoelectric crystal type	± 0.5
Voltage	0–250 kS/s	± 50 ppm of sample rate	Voltages signals	± 0.5

3. Results and Discussion

3.1. Calibration of CVCC

A new combustion chamber was created to perform calibration for a combustion system. In this investigation, LPG was applied as a calibration gas. The CVCC was calibrated using the combustion characteristics of flame speed (chamber pressure, flame speed, flame propagation, and gross heat release rate). Figure 5 shows the flame speed of LPG at various ERs from 0.8 to 1.2. LPG had a fastest flame speed of 0.348 m/s at $\phi = 1$. When comparing the three and present works, the percentage error difference was around 22%.

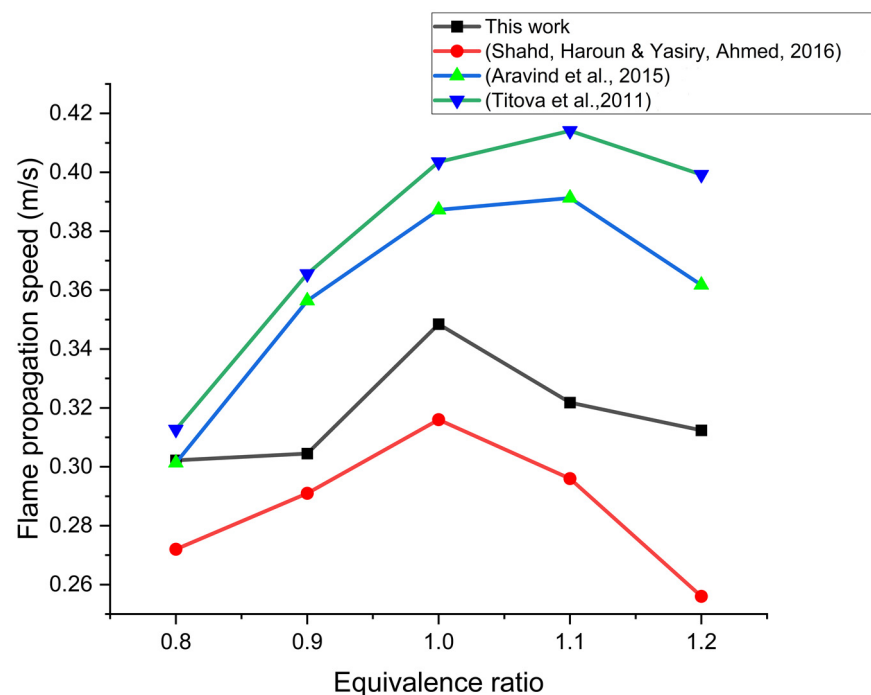


Figure 5. The calibration of flame propagation speed compared to other LPG experiments [25–27].

3.2. Combustion Characteristics of BPG

For an actual internal combustion engine to operate correctly, the flame shape must accurately depict the spatial distribution of the combustion flame. Table 4 displays the flame propagation of LPG and BPG (WP, CH, and PKS) when $\phi = 1.1$. The combustion photos were captured from the CVCC's front view using a high-speed camera (fps = 2000). Even if the photos occasionally displayed saturated flames, it was still possible to measure the flame geometry. Additionally, the images provided reliable information for comparing each fuel's combustion characteristics. The combustion process was started using an electrode positioned in the middle of the CVCC. Premixed combustion accounted for most of the combustion process, with the spark electrode serving as the primary source of flame brightness. Flameless combustion occurred due to the high water vapor content of the BPG in the gasifier. The combustion of the BPG lasted between 5 and 20 ms; the flame was dim and hazy, so an external semicircle and center point were drawn to improve appearance. For all fuels, due to the homogeneity of the fuel–air mixture in the CVCC, the flames expanded spherically from the center of the CVCC as combustion occurred. When considering the flame diameter, a more effective flame diameter indicated that flame propagation development for a given time was occurring more quickly.

Table 4. Images of flame propagation of LPG and BPG.

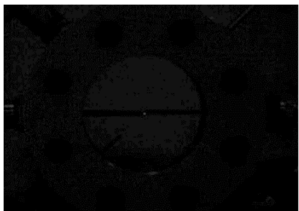
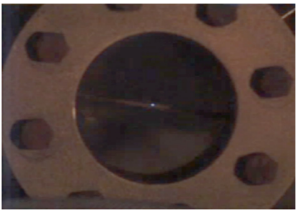
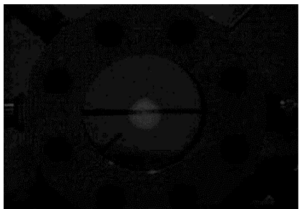
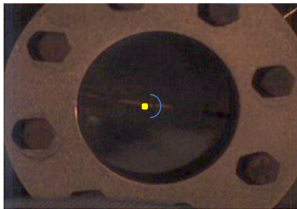
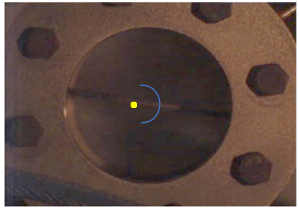
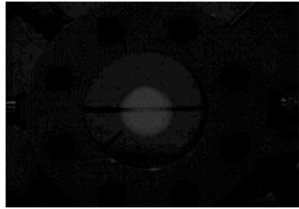
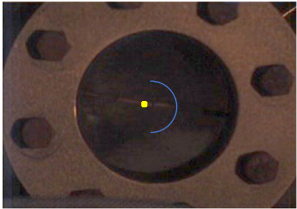
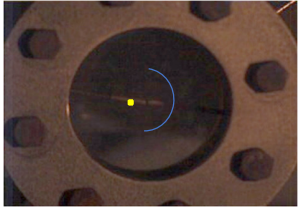
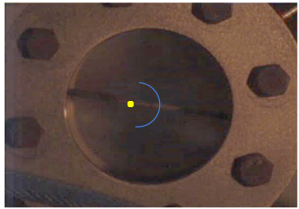
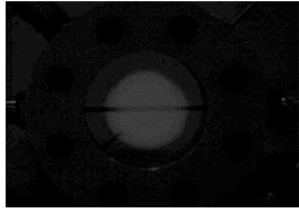
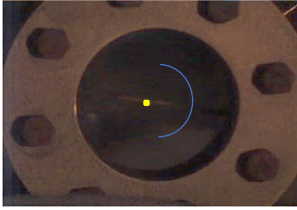
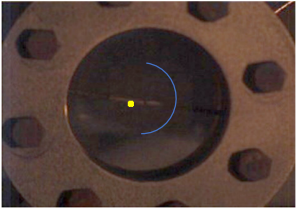
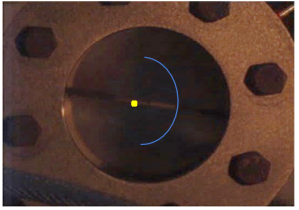
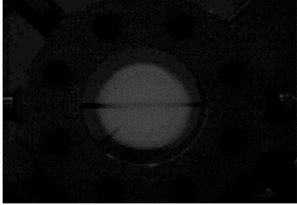
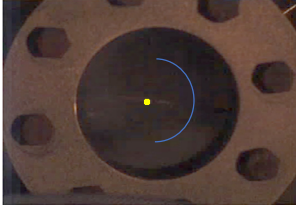
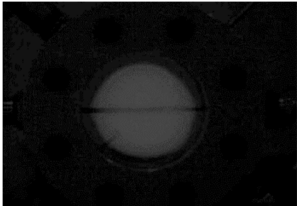
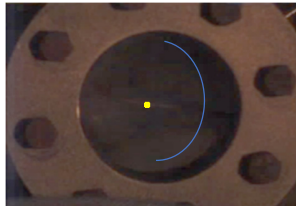
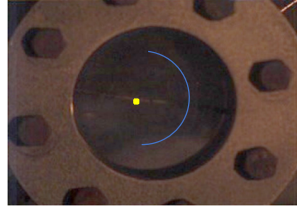
Time (ms)	LPG and BPG			
	LPG	WP	CH	PKS
0				
5				
10				
15				

Table 4. Cont.

Time (ms)	LPG and BPG			
	LPG	WP	CH	PKS
20				
25				

3.2.1. Chamber Pressure

Figure 6a–c demonstrate that the chamber pressure increased as the mixture approached the rich limits and decreased as it approaches the stoichiometric limit. The chamber pressure would drop if the ϕ was lean, which represented surplus air compared to a ϕ equal to 1. The chamber peak pressure of 21.55 bar was reached when the ϕ was stoichiometric ($\phi = 1$). Figure 6a depicts the peak pressure at a ϕ of 0.7 (approximately 20.24 bar). The chamber peak pressure was the lowest at 19.02 bar when the ϕ was 1.3. Lean conditions differed from stoichiometric conditions by about 6.07% while rich conditions differed by about 11.74%.

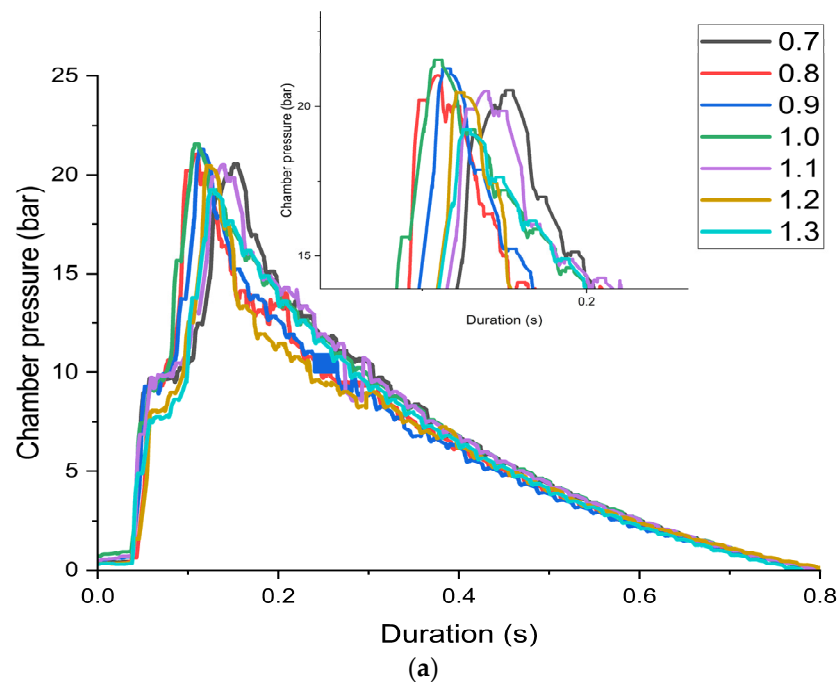


Figure 6. Cont.

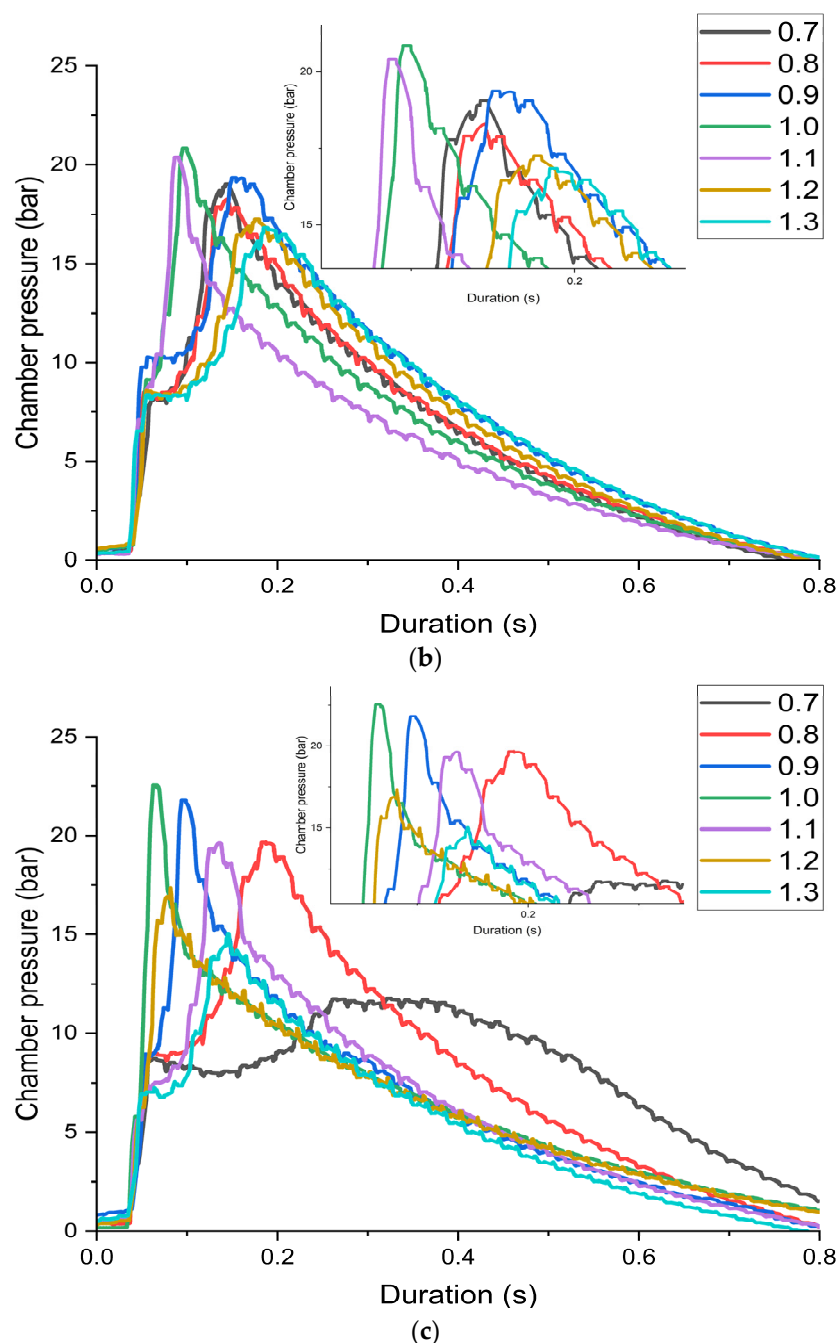


Figure 6. Chamber pressures of different BPGs at ϕ from 0.7 to 1.3: (a) WP; (b) CH; (c) PKS.

When the equivalence ratio was stoichiometric ($\phi = 1$), the maximum pressure of 20.84 bar was reached. The maximum pressure at a ϕ of 0.7, roughly 17.77 bar, is shown in Figure 6b. When the ϕ was 1.3, the chamber peak pressure had the lowest value at around 16.37 bar. Rich conditions deviated from stoichiometric at around 21.44% while lean conditions deviated by about 14.73%. The shortest time for combustion occurred when the ϕ was stoichiometric and the closest rich or lean situation followed after that.

The chamber peak pressure with a ϕ of 0.7 shown in Figure 6c was the lowest at 11.62 bar because the ϕ was rich, meaning there was a surplus of fuel and the pressure dropped due to incomplete combustion. The highest pressure was attained at around 22.54 bar when the ϕ was stoichiometric. When the ϕ was 1.3, the peak pressure was 15.03 bar, which decreased linearly to the rich condition. The period of combustion was the

shortest when the ϕ was stoichiometric and followed by the nearest rich or lean condition. When the ϕ was stoichiometric, it could show the premixed combustion shape.

The comparison of the peak pressure at the ϕ was stoichiometric based on Figure 6. The PKS had the highest peak pressure of 22.54 bar followed by WP at 21.55 bar, while CH had the lowest peak pressure of 20.84 bar. Comparatively, there was a difference of about 7.54% between the highest and lowest percentage.

3.2.2. HRR Analysis

HRR is a critical element in understanding laminar and turbulent responding flows. Examining the spatial distribution of heat release makes it feasible to identify flame propagation. Critical physical processes such as the interplay of flames and turbulence are directly impacted by this geographical distribution. This spatial distribution directly affects crucial physical processes such as the interaction between flames and turbulence, which interact to flames to cause combustion instabilities [28]. The combustion process requires a faster and more rapid increment in HRR because this will show a faster rate of air–fuel mixture combustion, which improves engine efficiency. It was found that the combustion process in a CVCC was represented by the first spike and a typically fluctuating curve that subsequently decayed. These findings demonstrated that the dominant combustion processes were premixed combustion as shown by the spike and diffusion ignition as shown by the HRR graph.

Figure 7a–c show the HRRs of different BPGs. Compared to when the ϕ was stoichiometric, the largest HRR was 140 kW when the ϕ was 1.1, but the time to achieve the HRR was the longest. The HRR at a ϕ equal to 1 was 133 kW compared to the highest HRR, which was a ϕ of 1.1, which differed by approximately 5.12%. Compared to lean and rich conditions, the premixed combustion phase produced the smallest narrow shape when the ϕ was stoichiometric. A flame with a high HRR will radiate more energy compared to one with a low HRR [29]. Figure 7a shows that for a ϕ of 0.7, 0.8, 0.9, 1.0, 1.1, 1.2, and 1.3, the times required to achieve premixed combustion of WP were 0.032, 0.038, 0.033, 0.033, 0.034, 0.033, and 0.033 s, respectively. Regarding the time to achieve an HRR of ϕ ranging from 0.7 to 1.3, a ϕ of 0.8 was the longest at around 0.038 ms.

The maximum HRR occurred at 119 kW when the ϕ was 0.9. The HRR at a ϕ of 1.1 was 102 kW, which differed from the highest HRR at a ϕ of 0.9 of about 10.23%. When the ϕ was 0.9, the premixed combustion phase produced the least narrow shape compared to the lean and rich situations. Figure 7b shows that at a ϕ of 0.7, 0.8, 0.9, 1.0, 1.1, 1.2, and 1.3, the times required to achieve premixed combustion of the CH were around 0.031, 0.030, 0.028, 0.029, 0.028, 0.030, and 0.028 s, respectively. It took the period from 0.028 ms to 0.031 ms to reach the premixed condition at a ϕ of 0.7 to 1.3.

According to Figure 7c, the peak HRR for PKS was around 49.42, 54.57, 70.77, 150.70, 47.21, 83.34, and 56.21 kW for a ϕ of 0.7, 0.8, 0.9, 1.0, 1.1, 1.2, and 1.3, respectively. When the ϕ was stoichiometric, the maximum HRR was 149 kW. A period of 0.020 ms was required to reach an HRR of ϕ equal to 1. This graph illustrates that the highest HRR and quickest duration to HRR were obtained when the ϕ is equal to 1. The graph shows that for a ϕ of 0.7, 0.8, 0.9, 1.0, 1.1, 1.2, and 1.3, the period required to achieve premixed combustion of PKS was around 0.022, 0.022, 0.025, 0.019, 0.021, 0.022, and 0.020 s, respectively. The average period to achieve premixed combustion for ϕ ranging from 0.7 to 1.3 was around 0.021 ms, but a ϕ of 0.9 was the longest at 0.025 ms.

A comparison of the peak HRR at ϕ between 0.9 and 1.1 was conducted based on Figure 7. PKS had the highest peak HRR of 149 kW at a ϕ equal to 1 followed by WP at around 140 kW at a ϕ of 1.1, while CH had the lowest peak HRR of 119 kW at a ϕ of 0.9. The HRR curve calculated the rate of pressure change; the chamber pressure is one of the primary factors that affects the HRR. Comparatively, there was a percentage difference of about 20.13% between the highest and lowest values of HRR. Figure 7a–c show that the period required to achieve premixed combustion of PKS was the fastest at 0.019 s, while the slowest duration to achieve premixed combustion was held by the WP at about 0.038 s.

Regarding the duration to achieve the premixed combustion, in the comparison between PKS and WP, it was 43.92%.

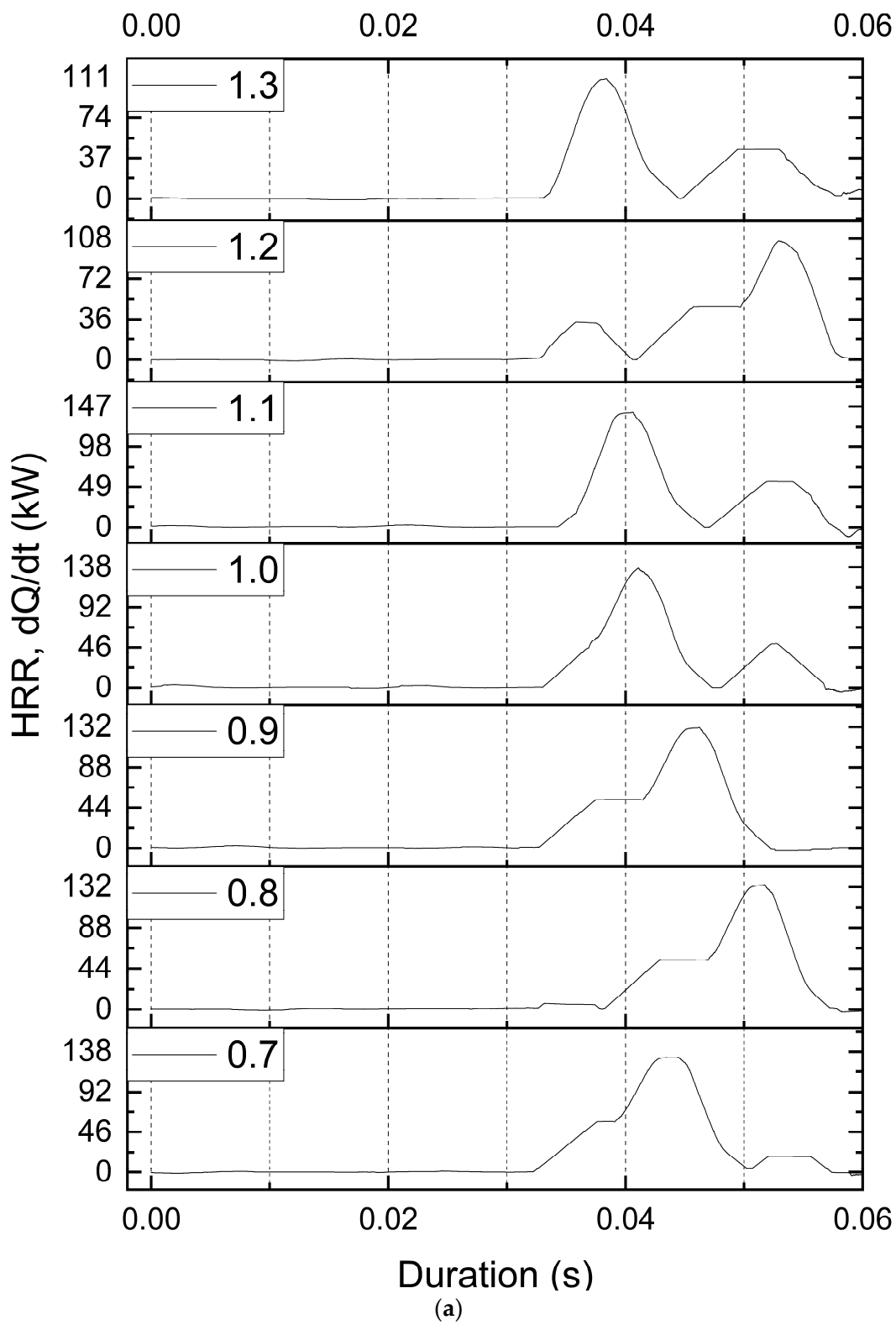


Figure 7. Cont.

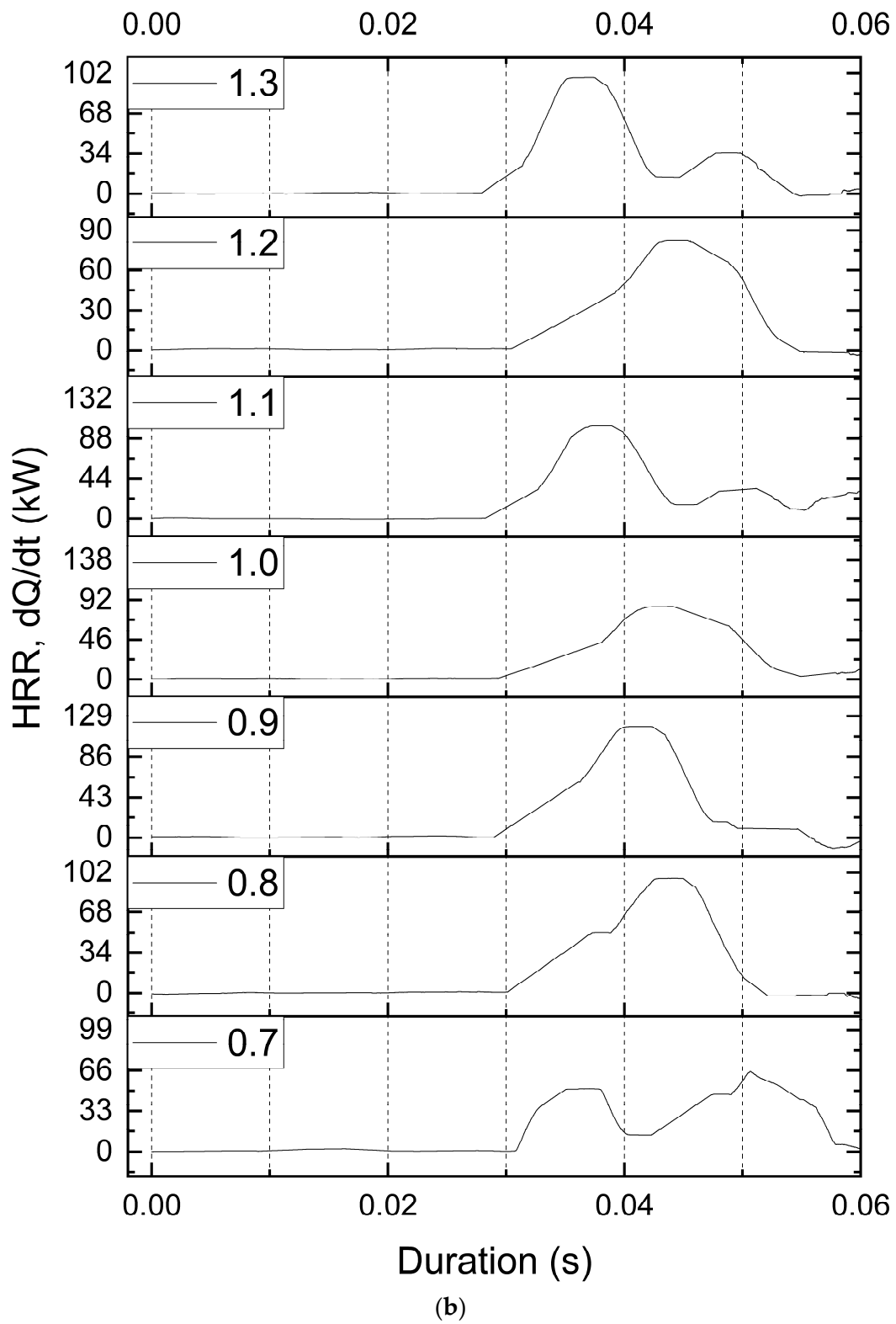


Figure 7. Cont.

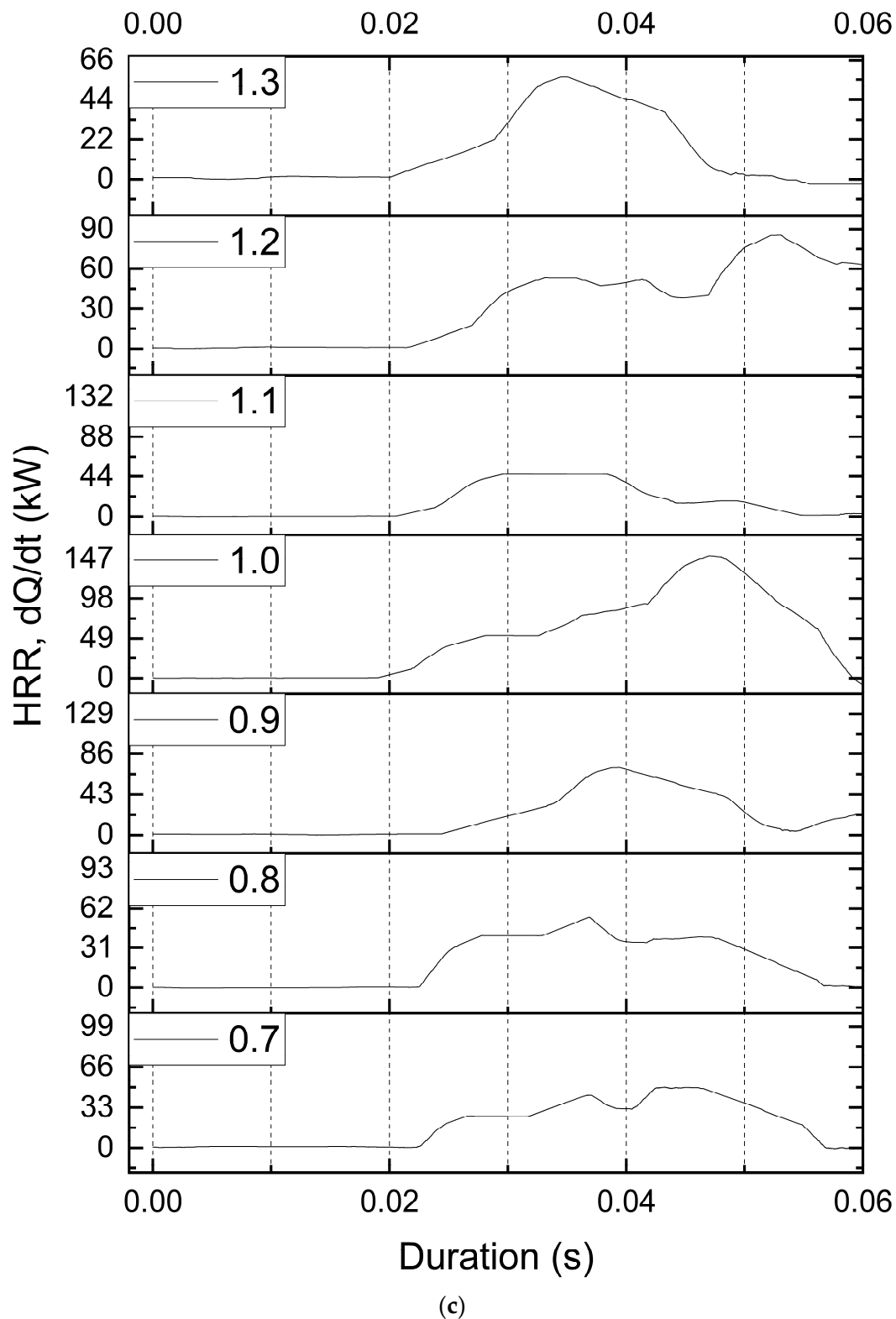


Figure 7. HRRs of different BPGs at ϕ from 0.7 to 1.3: (a) WP; (b) CH; (c) PKS.

3.2.3. Flame Propagation Speed

Figure 8 compares the fixed initial pressures for three different BPG–air mixtures with a ϕ ranging from 0.7 to 1.3. The graph demonstrates that the flame propagation speed increased as the combination approached the rich limits and decreases as it approached the

stoichiometric limit. The highest flame propagation speed determined by the study was obtained at a ϕ equal to 1.

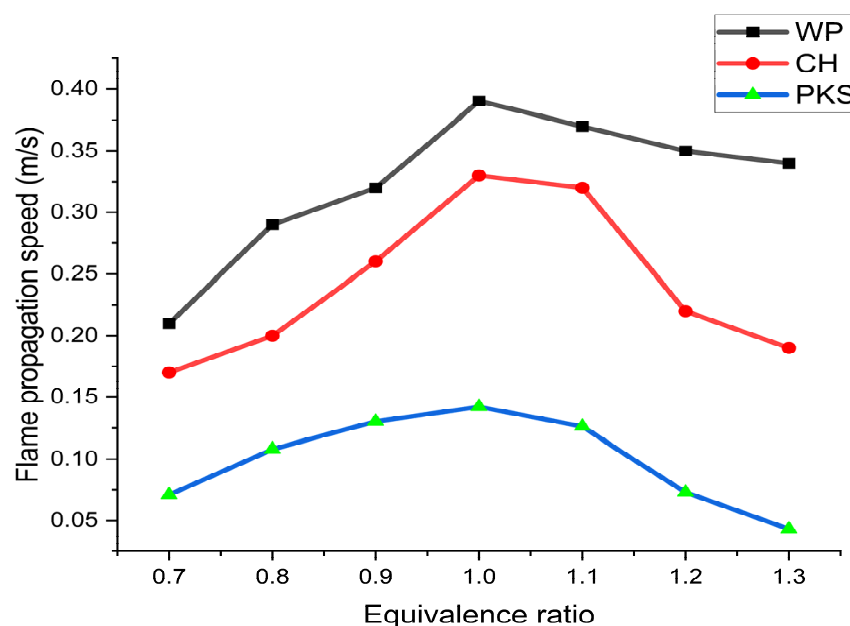


Figure 8. Flame propagation speed of 3 BPGs at ϕ from 0.7 to 1.3.

In comparison to those of the other two biomass feedstocks, the BPG of WP had the fastest flame propagation speed. When the ϕ was stoichiometric, WP had the fastest flame propagation speed of about 0.39 m/s whereas PKS was the slowest and only reached about 0.142 m/s, while the flame propagation speed of CH reached about 0.33 m/s. The higher concentration of hydrogen content of a BPG increased the flame propagation speed. The peak flame propagation speed of CH compared to PKS was around 15.38% while the peak flame propagation speed of CH compared to WP was approximately 63.58%.

3.2.4. Emissions of CO₂ and CO

The CO₂ and CO emission traces for the three BPG–air mixtures is shown in Figures 9 and 10, in which they are contrasted at fixed initial pressures with a ϕ ranging from 0.7 to 1.3. The BPG–air mixtures decreased as expected until the stoichiometric ϕ was equal to 1, then slightly increased after it reached 1, and then decreased linearly to the prosperous state. The complete burning resulted in more CO₂ being produced when the ϕ was stoichiometric. At a ϕ of 0.7, the CO₂ emissions for WP showed the maximum level of about 9.19% while the CO₂ emissions for CH showed the lowest level at 2.03%. The ultimate analysis of the biomass feedstock will have an impact on CO₂ emissions. Based on Table 3, the CO₂ composition of WP was 3.42% and the CO₂ composition of CH was around 2.93%. The CH₄ composition of WP was 0.77% and the CH₄ composition of CH was around 0.45%. The high carbon content of the biomass used as a producer gas will impact the CO₂ emissions. The CO emissions of WP reached their peak of about 0.196% at a ϕ of 0.7 whereas the CO emissions for CH reached the lowest level of 0.022%. While a ϕ of 1.2 showed an increase in CO in the rich condition, the emissions of CO decreased from the lean condition to the rich condition. Due to air shortage and reactant concentration in rich combinations, all the carbon could not be converted to CO₂ and instead formed a CO concentration. A tiny amount of CO was also released under lean conditions due to chemical kinetic effects even if the CO was created during operation in rich mixtures [30].

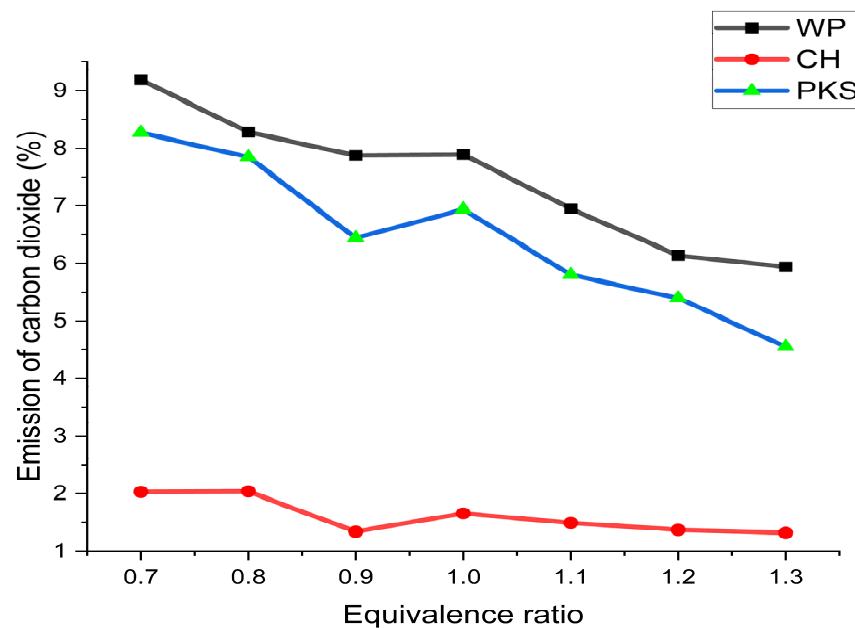


Figure 9. Emissions of carbon dioxide of 3 BPGs at ϕ from 0.7 to 1.3.

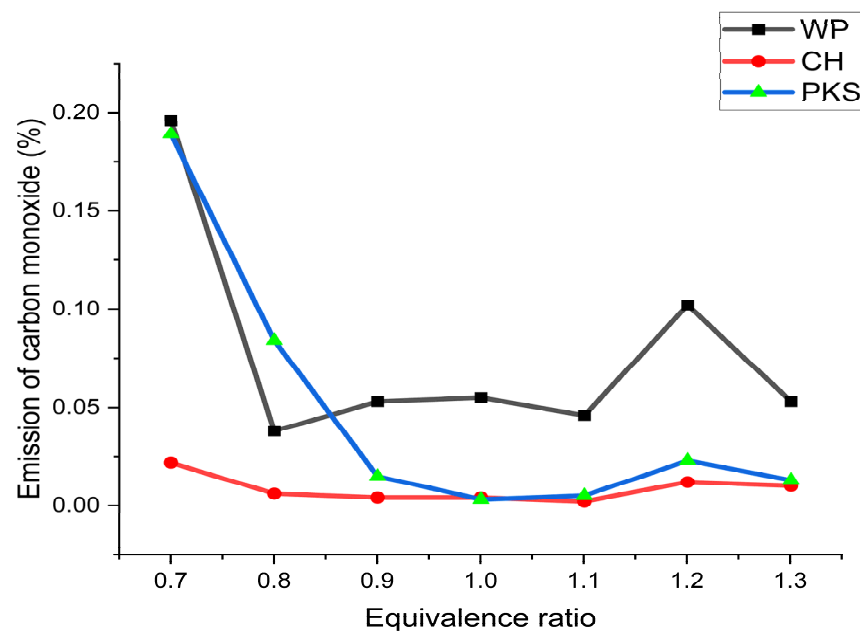


Figure 10. Emissions of carbon monoxide of 3 BPG at ϕ from 0.7 to 1.3.

4. Conclusions

Compared to other experimental findings, the calibration using the flame speed parameters was successful. The combustion characteristics of BPG were studied in a CVCC under various environmental conditions such as ambient temperature and pressure. The chamber pressure, flame propagation image, flame propagation speed, and emission gas were used to determine the characteristics of BPGs, which were compared in a similar temperature and pressure environment. Following is a summary of the results:

1. When the equivalence ratio was equal to 1, the chamber peak pressure of the three different forms of BPG reached its maximum. PKS has the highest chamber peak pressure of 22.54 bar, WP was second at around 21.55 bar, and CH had the lowest chamber peak pressure of 20.84 bar. On average, there was a gap of about 7.54% between the highest and lowest percentages. Due to the LHV, the CH has the lowest

- chamber peak pressure. The inference was that a biomass feedstock with a low LHV indicated low energy levels that lowered the chamber peak pressure.
- As the mixture approached the rich limits, the flame propagation speed increased and then decreased as it approaches the stoichiometric limit. The flame propagation speed of the PKS was the slowest, only reaching about 0.142 m/s, whereas that of the CH was about 0.33 m/s. WP had the fastest flame propagation speed, reaching roughly 0.39 m/s when the ϕ was stoichiometric. The flame propagated fastest because the WP had the highest LHV (1 MJ/Nm³). The peak flame propagation for CH was approximately 15.38% quicker than the peak flame propagation for PKS and 63.58% faster than the peak flame propagation for WP. The higher concentration of hydrogen content of the BPG would increase the flame propagation speed.
 - The BPG–air mixtures decreased as expected up to the stoichiometric ϕ equal to 1 and increased until they reached the rich condition and then decreased linearly. The burning process would produce more carbon dioxide when the ϕ was stoichiometric. The amount of carbon monoxide produced increased whether the ϕ was lean or rich. Although the ϕ of 1.2 showed an increase in CO in the rich condition, the emissions of CO decreased from the lean condition to the rich condition. Due to a shortage of air and reactant concentration in complicated mixtures, all the carbon could not be converted to CO₂; instead, a CO concentration was created. When comparing the three types of BPG, CH produced the lowest emissions of CO₂ and CO at 2.03% and 0.022%, respectively.

Author Contributions: Conceptualization, J.S.T.; Software, J.S.T. and Y.H.T.; Validation, J.S.T. and Y.H.T.; Formal analysis, J.S.T.; Resources, J.S.T. and Y.H.T.; Writing—original draft preparation, J.S.T. and Y.H.T.; Writing—review and editing, Y.H.T., H.G.H. and M.Y.I.; Visualization, J.S.T., Y.H.T. and M.Y.I.; supervision, Y.H.T., H.G.H. and H.T.N.; Project administration, J.S.T., Y.H.T. and T.D.L.; Funding acquisition, Y.H.T., M.Y.I., T.D.L. and H.T.N. All authors have read and agreed to the published version of the manuscript.

Funding: This study was supported and acknowledged by the Ministry of Higher Education Malaysia for Fundamental Research Grant Scheme under Project Code: FRGS/1/2019/TK07/USM/03/3 and Universiti Sains Malaysia Research University (RUI) under Grant Scheme 1001.PMEKANIK.8014136.

Data Availability Statement: Not applicable.

Acknowledgments: The authors would like to acknowledge the Universiti Sains Malaysia for financial support toward this study.

Conflicts of Interest: The authors declare no conflict of interest.

References

- Shahsavari, A.; Akbari, M. Potential of solar energy in developing countries for reducing energy-related emissions. *Renew. Sustain. Energy Rev.* **2018**, *90*, 275–291. [[CrossRef](#)]
- Dębowski, M.; Dudek, M.; Zieliński, M.; Nowicka, A.; Kazimierowicz, J. Microalgal Hydrogen Production in Relation to Other Biomass-Based Technologies—A Review. *Energies* **2021**, *14*, 6025. [[CrossRef](#)]
- Jha, S.; Nanda, S.; Acharya, B.; Dalai, A.K. A Review of Thermochemical Conversion of Waste Biomass to Biofuels. *Energies* **2022**, *15*, 6352. [[CrossRef](#)]
- Song, J.; Feng, R.; Yue, C.; Shao, Y.; Han, J.; Xing, J.; Yang, W. Reinforced urban waste management for resource, energy and environmental benefits: China's regional potentials. *Resour. Conserv. Recycl.* **2021**, *178*, 106083. [[CrossRef](#)]
- Sitka, A.; Jodkowski, W.; Szulc, P.; Smykowski, D.; Szumilo, B. Study of the Properties and Particulate Matter Content of the Gas from the Innovative Pilot-Scale Gasification Installation with Integrated Ceramic Filter. *Energies* **2021**, *14*, 7476. [[CrossRef](#)]
- Cerón, A.L.; Konist, A.; Lees, H.; Järvi, O. Effect of Woody Biomass Gasification Process Conditions on the Composition of the Producer Gas. *Sustainability* **2021**, *13*, 11763. [[CrossRef](#)]
- Karki, S.; Poudel, J.; Oh, S.C. Thermal Pre-Treatment of Sewage Sludge in a Lab-Scale Fluidized Bed for Enhancing Its Solid Fuel Properties. *Appl. Sci.* **2018**, *8*, 183. [[CrossRef](#)]
- Simsek, S.; Uslu, S. Comparative evaluation of the influence of waste vegetable oil and waste animal oil-based biodiesel on diesel engine performance and emissions. *Fuel* **2020**, *280*, 118613. [[CrossRef](#)]

9. Okolie, J.A.; Nanda, S.; Dalai, A.K.; Berruti, F.; Kozinski, J.A. A review on subcritical and supercritical water gasification of biogenic, polymeric and petroleum wastes to hydrogen-rich synthesis gas. *Renew. Sustain. Energy Rev.* **2019**, *119*, 109546. [[CrossRef](#)]
10. Mishra, S.; Upadhyay, R.K. Review on biomass gasification: Gasifiers, gasifying mediums, and operational parameters. *Mater. Sci. Energy Technol.* **2021**, *4*, 329–340. [[CrossRef](#)]
11. Awais, M.; Omar, M.M.; Munir, A.; Li, W.; Ajmal, M.; Hussain, S.; Ahmad, S.A.; Ali, A. Co-gasification of different biomass feedstock in a pilot-scale (24 kWe) downdraft gasifier: An experimental approach. *Energy* **2022**, *238*, 121821. [[CrossRef](#)]
12. Feng, M.; Xin, L.; Wang, Z.; Li, K.; Wu, J.; Li, J.; Cheng, W.; Wang, B. Discussion on requirements of gasifier gas tightness for underground coal gasification production. *Sustain. Energy Technol. Assessments* **2021**, *47*, 101550. [[CrossRef](#)]
13. AlNouss, A.; McKay, G.; Al-Ansari, T. Enhancing waste to hydrogen production through biomass feedstock blending: A techno-economic-environmental evaluation. *Appl. Energy* **2020**, *266*, 114885. [[CrossRef](#)]
14. Commeh, M.K.; Kemausuor, F.; Badger, E.N.; Osei, I. Experimental study of ferrocement downdraft gasifier engine system using different biomass feedstocks in Ghana. *Sustain. Energy Technol. Assessments* **2019**, *31*, 124–131. [[CrossRef](#)]
15. Kohli, R. *Applications of Solid Carbon Dioxide (Dry Ice) Pellet Blasting for Removal of Surface Contaminants*; Elsevier Inc.: Amsterdam, The Netherlands, 2018.
16. Zeng, W.; Liu, J.; Ma, H.; Liu, Y.; Liu, A. Experimental study on the flame propagation and laminar combustion characteristics of landfill gas. *Energy* **2018**, *158*, 437–448. [[CrossRef](#)]
17. Wang, Y.; Wang, H.; Meng, X.; Tian, J.; Wang, Y.; Long, W.; Li, S. Combustion characteristics of high pressure direct-injected methanol ignited by diesel in a constant volume combustion chamber. *Fuel* **2019**, *254*, 115598. [[CrossRef](#)]
18. Agarwal, A.K.; Jiotode, Y.; Sharma, N. Endoscopic visualization of engine combustion chamber using diesoline, diesosene and mineral diesel for comparative spatial soot and temperature distributions. *Fuel* **2018**, *241*, 901–913. [[CrossRef](#)]
19. Lee, C.-F.; Pang, Y.; Wu, H.; Nithyanandan, K.; Liu, F. An optical investigation of substitution rates on natural gas/diesel dual-fuel combustion in a diesel engine. *Appl. Energy* **2020**, *261*, 114455. [[CrossRef](#)]
20. Carlucci, A.; de Risi, A.; Laforgia, D.; Naccarato, F. Experimental investigation and combustion analysis of a direct injection dual-fuel diesel–natural gas engine. *Energy* **2008**, *33*, 256–263. [[CrossRef](#)]
21. Homdoun, N.; Tippayawong, N.; Dussadee, N. Prediction of small spark ignited engine performance using producer gas as fuel. *Case Stud. Therm. Eng.* **2015**, *5*, 98–103. [[CrossRef](#)]
22. Thangaiyan, A.K.; Ibrahim, M.M.M. Production of producer gas and its use as the supplementary fuel for SI engine. *Biomass Convers. Biorefinery* **2021**, *11*, 1–9. [[CrossRef](#)]
23. Ram, N.K.; Singh, N.R.; Raman, P.; Kumar, A.; Kaushal, P. A detailed experimental analysis of air–steam gasification in a dual fired downdraft biomass gasifier enabling hydrogen enrichment in the producer gas. *Energy* **2019**, *187*, 115937. [[CrossRef](#)]
24. Baruah, D.; Kalita, P.; Moholkar, S. *A Comprehensive Study on Utilization of Producer Gas as IC Engine Fuel*; Springer: Berlin/Heidelberg, Germany, 2021.
25. Steinberg, A.M.; Hamlington, P.E.; Zhao, X. Structure and dynamics of highly turbulent premixed combustion. *Prog. Energy Combust. Sci.* **2021**, *85*, 100900. [[CrossRef](#)]
26. Shahad, H.A.K.; Yasiry, A.S. An Experimental Study for Investigating the Laminar Flame Speed and Burning Velocity for LPG. *Int. J. Therm. Technol.* **2016**, *6*, 7–12.
27. Aravind, B.; Kishore, V.R.; Mohammad, A. Combustion characteristics of the effect of hydrogen addition on LPG-air mixtures. *Int. J. Hydrogen Energy* **2015**, *40*, 16605–16617. [[CrossRef](#)]
28. Titova, N.S.; Kuleshov, P.S.; Starik, A.M. Kinetic mechanism of propane ignition and combustion in air. *Combust. Explos. Shock Waves* **2011**, *47*, 249–264. [[CrossRef](#)]
29. Liu, Y.; Tan, J.; Wang, H.; Lv, L. Characterization of heat release rate by OH* and CH* chemiluminescence. *Acta Astronaut.* **2018**, *154*, 44–51. [[CrossRef](#)]
30. Reşitoğlu, İ.A.; Altinişik, K.; Keskin, A. The pollutant emissions from diesel-engine vehicles and exhaust aftertreatment systems. *Clean Technol. Environ. Policy* **2015**, *17*, 15–27. [[CrossRef](#)]